Acta. Chim. Asiana., 2025, 8(1), 612-622
e-ISSN/p-ISSN 2550-0503/2550-049x
Available online at: www.aca.unram.ac.id

RESEARCH PAPER

Eco-friendly designing of zinc oxide nanoparticle as a potential semiconducting device for H_2O-capture: A density functional theory study

Fatemeh Mollaamin[a*]

[a] Department of Biomedical Engineering, Faculty of Engineering and Architecture, Kastamonu University, Kastamonu, Turkey
E-mail: fmollaamin@kastamonu.edu.tr

DOI: 10.29303/aca.v8i1.233

Article info:

Received 24/01/2025

Revised 03/03/2025

Accepted 06/03/2025

Available online 30/05/2025

Abstract: We employ first-principles calculations to investigate the structural stability and electronic properties of zinc oxide (ZnO) nanocluster adsorbed with H_2O molecule. A comprehensive investigation on H_2O grabbing by ZnO nanocluster was carried out using DFT computations at the CAM–B3LYP–D3/6–311+G (d, p) level of theory. The hypothesis of the energy adsorption phenomenon was confirmed by density distributions of CDD, TDOS/PDOS/OPDOS, and ELF for ZnO and ZnO–H_2O. A vaster jointed area engaged by an isosurface map for H/OH adsorption on ZnO surface towards formation of ZnO–H_2O complex due to labeling atoms of O1, Zn15, O27, H29, H30. Therefore, it can be considered that zinc in the functionalized ZnO might have more impressive sensitivity for accepting the electrons in the process of H/OH adsorption. It is considerable that when all surface atoms of ZnO are coated by OH and H groups, the semiconducting behavior is recovered. Our results open up the possibility of tailoring the electronic properties by controlling the surface adsorption sites. The nanoclusters of bare ZnO and ZnO–H_2O can be defined by ELF graphs owing to exploring their delocalization/localization characterizations of electrons and chemical bonds. The results indicate that the stability and the optical gap are related to the sizes and symmetries of the clusters. Further, it is shown that the structures have much greater impact on the optical gap, there is the dipole-forbidden transition in the optical gap for high symmetric structures.

Keywords: ZnO nanocluster; semiconductor; H/OH; adsorption; first principles

Citation: Mollaamin, F. 2025. Eco-friendly designing of zinc oxide nanoparticle as a potential semiconducting device for H2O-capture: a density functional theory study. *Acta Chimica Asiana*, 8(1), 612–622. https://doi.org/10.29303/aca.v8i1.233

INTRODUCTION

ZnO is a promising semiconductor material for various applications ranging from optoelectronics to biomedicine, attributed to its wide direct band gap, high exciton binding energy, high mobility, and high quantum efficiency. To further improve the performance of ZnO devices, plasma treatment is a common method for surface modification [1–4]. The luminescence properties of ZnO after plasma treatment are significantly changed, including ultraviolet (UV) luminescence, visible luminescence, and recombination mechanism [5–11].

Optical properties are improved significantly by H plasma, with negligible alteration in thickness. Although no chemical reaction is introduced, emission intensity is enhanced by Ar plasma by eliminating the non-radiative recombination centers. Furthermore, H and Ar plasma also induce strong exciton localization, leading to significant broadening of the UV spectrum [12–15].

However, replicating or applying the reported improvement in plasma treatments for ZnO often proves challenging. This difficulty arises from several factors, including the diverse properties of ZnO samples, which encompass thin films, single crystals and nanostructures grown through various methods. Moreover, the specific effects of plasma treatments using different gases remain unclear, as each type of gas plasma exhibits unique interactions. Consequently, it is crucial to conduct a systematic comparison of the influence of various plasma gases on the optical and electrical properties and to accurately identify the specific defects affected [16–21].

Transparent, superhydrophilic materials are indispensable for their self-cleaning function, which has become an increasingly popular research topic, particularly in photovoltaic (PV) applications. It was reported hydrophilic and superhydrophilic ZnO by varying the morphology for use as a self-cleaning coating for PV applications [22].

The researchers have applied molecular dynamics simulations through a reactive force-field for ZnO–H_2O ambient. The force-field parameters were fitted to a dataset of energies, geometries and charges derived from density functional theory calculations. The applied model has provided a good fit to the quantum mechanics reference data for the ZnO–H_2O system that was present in the dataset. The force-field has been used to study how H_2O is adsorbed, molecularly or dissociatively, at monolayer coverage on flat and stepped ZnO surfaces, at different temperatures. The results show that structures that promote hydrogen bonding are favored and that the presence of steps promotes an increased level of hydroxylation in the water monolayers [23].

In this work, we analyzed the effect of H_2O adsorption on the properties of ZnO nanocluster via the density of state, charge distribution, bond orders and HOMO–LUMO orbitals using DFT studies. The optimized ZnO is shown in Figure 1, and the Zn and O atoms are also numbered to characterize the reaction pathway.

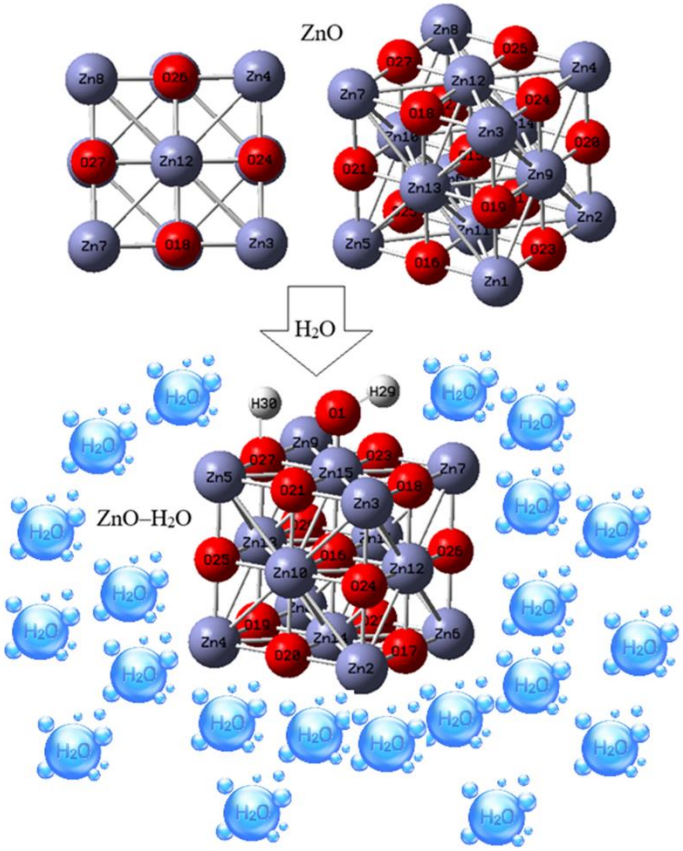

Figure 1. Characterization of bare ZnO and ZnO–H_2O nanoclusters through a labeled ring in clockwise manner including H, O, Zn towards H_2O -adsorption.

In this work, the ZnO–H_2O sensor was successfully labeled for the detection of relative humidity by employing nearest neighbor analysis. The adsorbing mechanisms

of water molecules on the ZnO surface were also investigated by using the density functional theory.

THEORY, MATERIALS AND COMPUTATION

The hydration of ZnO with 27 atoms and formation of ZnO–H_2O complex with 30 atoms were calculated within the framework of first-principles calculation based on density functional theory (DFT) (Figure1) through multiplicity=1 and convergence= 0.6367D-08. The rigid potential energy surface using density functional theory [24–37] was performed due to Gaussian 16 revision C.01 program package [38] and GaussView 6.1 [39]. The coordination input for energy storage on the solar cells has applied 6–311+G (d,p) and EPR–3 basis sets.

First, we optimized the structural parameters of the nanocluster of bare ZnO and hydrated nanocluster of ZnO–H_2O for obtaining the highest short-circuit current density. Figure 1 shows the process of H_2O-adsorption on nanocluster of bare ZnO which is varied to maximize the absorption in the active region. This is a utility used to calculate ring area and perimeter, since ring area is sometimes involved in wavefunction analysis. In this function, it is needed to input the index of the atoms in the ring in clockwise manner which can conclude the total ring area and total ring perimeter for a tailored ring as 9.4242 Å and 12.2796 $Å^2$, respectively (Figure1).

RESULTS AND DISCUSSION

In this article, the data has evaluated the efficiency of ZnO in H_2O medium through energies, geometries and charges derived from density functional theory calculations. The applied model has provided a good fit to the quantum mechanics reference data for the ZnO–H_2O system that was present in the dataset. The force-field has been used to study how water is adsorbed, molecularly at monolayer coverage on ZnO surface.

The amounts of charge density differences "CDD" is measured by considering isolated atoms or noninteracting ones. The mentioned approximation can be the lightest to use because the superposition value may be received from the primary status of the self-consistency cycle in the code that carries out the density functional theory (Figure2a, b) [40]. Figure2a indicates all Zn or O atoms of ZnO fluctuating around –9 to –1 Bohr. In Figure 2b, the atom of Zn15, O27 from ZnO–H_2O and O1, H29, H30 from H_2O molecule accompanying other Zn or O atoms from ZnO–H_2O have shown the fluctuation around –1 to +1 Bohr and –9 to +1 Bohr, respectively. Furthermore, atomic charge was discussed during H_2O adsorption by ZnO towards formation of ZnO–H_2O (Table1).

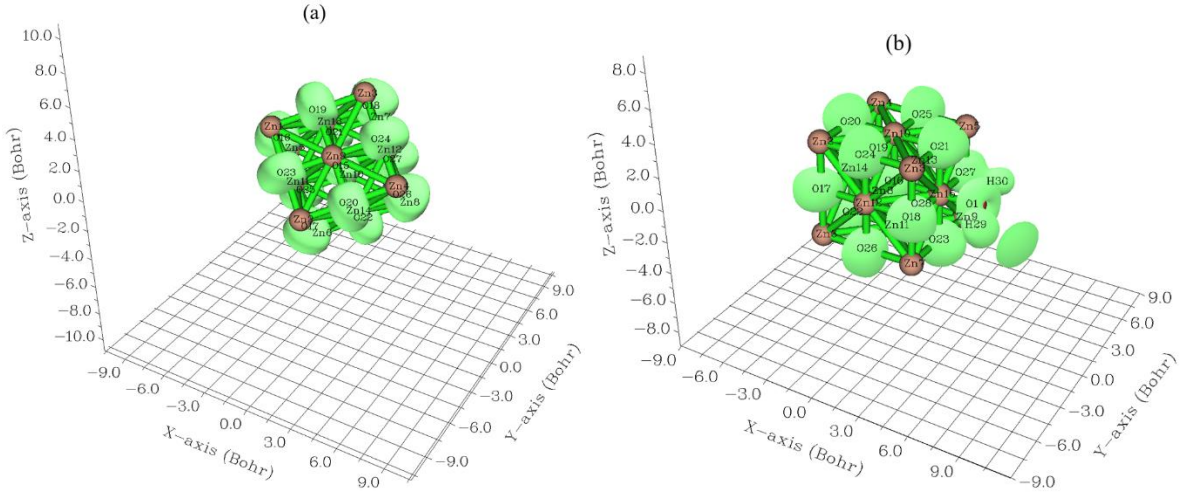

Figure2. CDD graphs for nanoclusters of (a) bare ZnO, and (b) ZnO–H_2O.

Table 1. The atomic charge (Q/coulomb) for bare ZnO and ZnO–H_2O nanoclusters.

Bare ZnO		ZnO–H_2O	
Atom	Charge	Atom	Charge
Zn1	0.7141	O1	–0.5958
Zn2	0.7139	Zn2	0.6972
Zn3	0.7135	Zn3	0.7278
Zn4	0.7141	Zn4	0.7273
Zn5	0.7141	Zn5	0.5927
Zn6	0.7135	Zn6	0.6958
Zn7	0.7140	Zn7	0.7113
Zn8	0.7140	Zn8	0.7264
Zn9	1.7451	Zn9	0.5981
Zn10	1.7450	Zn10	1.7256
Zn11	1.7471	Zn11	1.7376

Bare ZnO		ZnO–H_2O	
Zn12	1.7471	Zn12	1.8835
Zn13	1.7461	Zn13	1.9004
Zn14	1.7460	Zn14	1.6986
O15	–1.5357	Zn15	1.4867
O16	–1.2210	O16	–1.5460
O17	–1.2210	O17	–1.2236
O18	–1.2210	O18	–1.2143
O19	–1.2209	O19	–1.2232
O20	–1.2209	O20	–1.2259
O21	–1.2209	O21	–1.1381
O22	–1.2209	O22	–1.2260
O23	–1.2210	O23	–1.1370
O24	–1.2210	O24	–1.2155
O25	–1.2210	O25	–1.2183
O26	–1.2210	O26	–1.2157
O27	–1.2210	O27	–1.1850
		O28	–1.2183
		H29	0.2973
		H30	0.3764

The atomic charge of Zn, O, and H/OH adsorbed on ZnO have been measured. The values detect that with adding H_2O, the negative atomic charge of oxygen atoms of O16, O 17, O18, O19, O20, O21, O22, O23, O24, O25, O26, O27, O28 in ZnO–H_2O has changed through coating of ZnO with H/OH adsorption. In fact, ZnO–H_2O has shown more efficiency than bare ZnO for admitting the electron from electron donor of O16 to O28 (Table 1 and Figure 3).

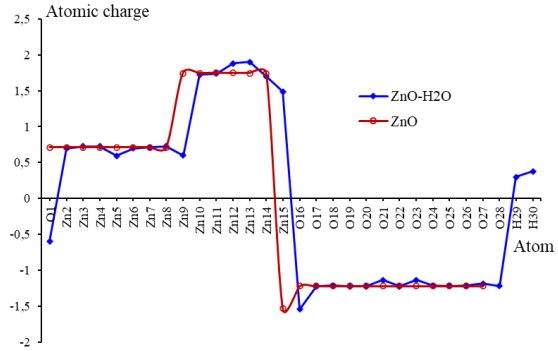

Figure3. The fluctuation of atomic charge (Q/coulomb) for ZnO and ZnO–H_2O nanoclusters.

The changes of charge density analysis in the adsorption process have illustrated that ZnO and ZnO–H_2O nanoclusters have shown the "Bader charge" of –1.747 and –1.900 coulomb, respectively. The differences of charge density for these structures are measured as: $\Delta Q_{ads.}$ = – 0.153 coulomb.

The dependence of electron-transfer rate constants on the driving force for interfacial charge transfer has been investigated using n-type ZnO electrodes in aqueous solutions. Differential capacitance versus potential and current density versus potential measurements were used to determine the energetics and kinetics, respectively, of the interfacial electron-transfer processes. All rate processes were observed to be kinetically first order in the concentration of surface electrons and first-order in the concentration of dissolved redox acceptors. The agreement between the reorganization energy of the ions in solution and the reorganization energy for the interfacial electron-transfer processes indicated that the reorganization energy was dominated by the redox species in the electrolyte, as expected from an application of Marcus theory to semiconductor electrodes.

To better understand the different adsorption characteristics of ZnO and ZnO–H_2O nanoclusters, total density of states (TDOS) using Multiwfn program [41,42] has been measured.

This parameter can indicate the existence of important chemical interactions often on the convex side (Figure 4a, b). In isolated system (such as molecule), the energy levels are discrete, the concept of density of state (DOS) is supposed completely valueless in this situation. Therefore, the original total DOS (TDOS) of isolated system can be written as [43]:

$$TDOS\ (E) = \sum_i \delta\ (E - \epsilon_i\ ) \qquad (1)$$

$$G(x) = \frac{1}{c\sqrt{2\pi}} e^{-\frac{x^2}{2c^2}}$$

where

$$c = \frac{\mathrm{FWHM}}{2\sqrt{2\ln x}} \qquad (2)$$

Moreover, the curve map of broadened partial DOS (PDOS) and overlap DOS (OPDOS) are valuable for visualizing orbital composition analysis, PDOS function of fragment *A* is defined as:

$$zPDOS_A\ (E) = \sum_i \Xi_{i,A}\ F\ (E - \epsilon_i\ ) \qquad (3)$$

where $\Xi_{i,A}$ is the composition of fragment *A* in orbital *i*. The OPDOS between fragment *A* and *B* is defined as:

$$OPDOS_{A,B}\ (E) = \sum_i X^i_{A,B}\ F\ (E - \epsilon_i\ ) \qquad (4)$$

where $X^i_{A,B}$ is the composition of total cross term between fragment *A* and *B* in orbital *i*.

In the TDOS map, each discrete vertical line corresponds to a molecular orbital (MO), the dashed line highlights the position of HOMO. The curve is the TDOS simulated based on the distribution of MO energy levels. In the negative part, the region around –0.60 to –0.80 a.u. has obviously larger state density

than other regions for ZnO and ZnO–H_2O nanoclusters (Figure 4a, b).

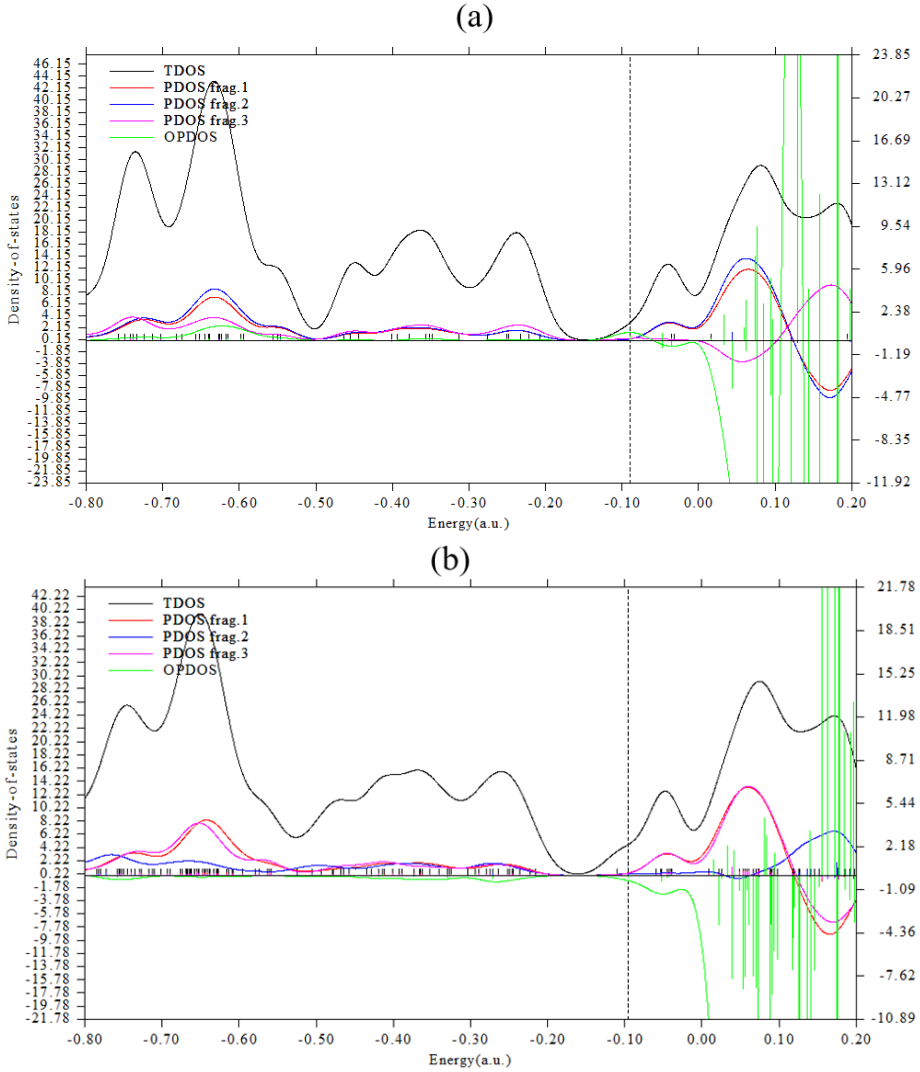

Figure 4. TDOS/PDOS/OPDOS graphs of nanoclusters of (a) bare ZnO, and (b) ZnO–H_2O.

However, it has bee has shown a larger state density through pointed peaks for ZnO–H_2O (Figure 4b) than ZnO (Figure4a) around –0.20 to –0.40 a.u. It is remarkable that when all surface atoms of ZnO are coated by OH and H groups, the semiconducting behavior is recovered. Our results open up the possibility of tailoring the electronic properties by controlling the surface adsorption sites.

Fragment 1 has been defined for Zn1 (Figure4a), O1 (Figure 4b) and Zn2, Zn4, Zn6, Zn8, Zn10, O16, O19, O22, O24 (Figure 4a, b) and H30 (Figure 4b). Moreover, Fragment 2 has indicated the fluctuation of Zn11, Zn12, Zn13, Zn14, O17, O25, O26, O27 for ZnO and ZnO–H_2O nanoclusters (Figure 4a, b) and H29 for ZnO–H_2O (Figure 4b). Finally, it was considered the fluctuation of O15 (Figure4a), Zn15 (Figure 4b) and Zn3, Zn5, Zn7, Zn9, O18, O20, O21, O23 for both ZnO and ZnO–H_2O nanoclusters (Figure 4a, b) through Fragment 3.

Furthermore, a type of scalar fields called electron localization function (ELF) may demonstrate a broad span of bonding samples. Nevertheless, the distinction between deduced/raised electron delocalization/localization into cyclic π-conjugated sets stays encouraging for ELF [44]. The grosser the electron localization is in an area, the more likely the electron movement is restricted within it. Therefore, they might be discerned from the ones away if electrons are totally centralized. As Bader investigated, the zones with large electron localization possess extensive magnitudes of Fermi hole integration. But, with having a six-dimension function for the Fermi hole, it seems hard to be studied directly. Then, Becke and Edgecombe remarked that spherically averaged like spin conditional pair probability

Acta. Chim. Asiana., 2025, 8(1), 612 – 622

possesses a direct correlation with the Fermi hole and proposed the parameter of electron localization function (ELF) in Multiwfn program [41,42] and popularized for spin-polarized procedure [45]:

$$\mathrm{ELF(r)} = \frac{1}{1+[D(\mathrm{r})/D_0(\mathrm{r})]} \quad (5)$$

where

$$D(\mathrm{r}) = \frac{1}{2}\sum_i \eta_i |\nabla\varphi_i(\mathrm{r})|^2 - \frac{1}{8}\left[\frac{|\nabla\rho_\alpha(\mathrm{r})|^2}{\rho_\alpha(\mathrm{r})} + \frac{|\nabla\rho_\beta(\mathrm{r})|^2}{\rho_\beta(\mathrm{r})}\right] \quad (6)$$

and $D_0(\mathrm{r}) = \frac{3}{10}(6\pi^2)^{2/3}\left[\rho_\alpha(\mathrm{r})^{5/3} + \rho_\beta(\mathrm{r})^{5/3}\right]$ (7)

For close-shell system, since $\rho_\alpha = \rho_\beta = (1/2)\rho$, *D* and D_0 terms can be simplified as:

$$D(\mathrm{r}) = \frac{1}{2}\sum_i \eta_i |\nabla\varphi_i(\mathrm{r})|^2 - \frac{1}{8}\frac{|\nabla\rho(\mathrm{r})|^2}{\rho(\mathrm{r})} \quad (8)$$

and

$$D_0(\mathrm{r}) = (3/10)(3\pi^2)^{2/3}\rho(\mathrm{r})^{5/3} \quad (9)$$

Regarding kinetic energy, ELF was rechecked to be more punctual for both Kohn-Sham DFT and post-HF wavefunctions [46]. In fact, the excess kinetic energy density caused by Pauli repulsion was unfolded by D(r) and D_0(r) may be inspected as Thomas-Fermi kinetic energy density. Because D_0(r) is brough forward the ELF as origin, what the ELF shows is an affiliate localization. The nanoclusters of bare ZnO and ZnO–H_2O can be defined by ELF graphs owing to exploring their delocalization/localization characterizations of electrons and chemical bonds (Figure 5a, b).

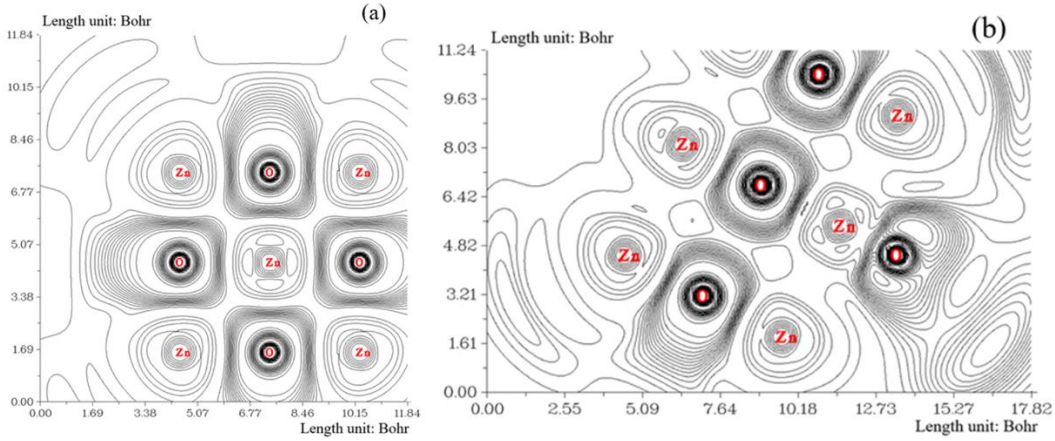

Figure 5. The counter map graphs of ELF for of nanoclusters of (a) bare ZnO, and (b) ZnO–H_2O.

The counter map of ELF for bare ZnO (Figure 5a) and ZnO–H_2O (Figure 5b) has shown the electron delocalization through H/OH adsorption (Figure5a, b). ZnO–H_2O nanocluster indicates a larger isosurface map of electron delocalization due to labeling atoms of O1, Zn15, O27, H29, H30. A narrower connected area occupied by an isosurface map means that electron delocalization is relatively difficult. However, the large counter map of ELF for ZnO–H_2O can confirm that ZnO can be a promising semiconductor material for various applications.

Moreover, intermolecular orbital overlap integral is important in discussions of intermolecular charge transfer which can calculate HOMO-HOMO and LUMO-LUMO overlap integrals between the H/OH and nanocluster of ZnO. The applied wavefunction level is CAM–B3LYP–D3/6–311+G (d, p) that correspond to HOMO and LUMO, respectively (Table2).

Table2. LUMO, HOMO, and energy gap (ΔE) for bare ZnO and ZnO–H_2O nanoclusters.

Nanoclusters	**bare ZnO**	**ZnO–H_2O**
E_{HOMO} (eV)	–2.4280	–2.6110
E_{LUMO} (eV)	–1.3056	–1.6053
$\Delta E=E_{LUMO}-E_{HOMO}$ (eV)	1.1223	1.0056

The differences between the HOMO-LUMO gap (delta(h-l)) and the optical gap (delta(opt)) are dramatic for small clusters (2 < or = n < or = 5). As the increasing of the cluster size, the differences become small. The results indicate that the stability and the optical gap are related to the sizes and symmetries of the clusters. Further, it is shown that the structures have much greater impact on the optical gap, there is the dipole-forbidden transition in the optical gap for high symmetric structures.

The amount of "Mayer bond order" [47] is generally according to empirical bond order for the single bond is nearly 1.0. "Mulliken bond

order" [48] with a small accord with empirical bond order is not appropriate for quantifying bonding strength, for which Mayer bond order always performs better. However, "Mulliken bond order" is a good qualitative indicator for "positive amount" of bonding and "negative amount" of antibonding which are evacuated and localized, respectively (Table 3).

Table 3. The bond order of Mayer, Wiberg, Mulliken, Laplacian and Fuzzy from mixed alpha and beta density matrix for ZnO through H/OH adsorption and formation of ZnO–H_2O nanocluster.

Bond order	Mayer	Wiberg	Mulliken	Laplacian	Fuzzy
O1–Zn15	1.1308	1.7176	1.9120	1.6451	1.6561
O1–H29	0.6507	0.6631	0.1727	0.2169	0.6878
O27–H30	0.4783	0.4490	0.0573	0.1505	0.4321

As it is seen in Table 3, “Laplacian bond order” [49] has a straight cohesion with bond polarity, bond dissociation energy and bond vibrational frequency. The low value of Laplacian bond order might demonstrate that it is insensitive to the calculation degree applied for producing electron density. Generally, the value of “Fuzzy bond order” is near Mayer bond order, especially for low-polar bonds, but much more stable with respect to the change in basis-set. Computation of “Fuzzy bond order” demands running “Becke's DFT” numerical integration, owing to which the calculation value is larger than assessment of “Mayer bond order” and it can concede more precisely [50]. Contrary to “Mayer bond order”, Mulliken's overlap population assigns a part of the electronic charge directly to the pair of atoms considered. It characterizes the accumulation of the electrons in the region between the chemically bonded atoms and is a very useful quantity often characterizing well the bond strength. However, it cannot be called bond order, because it does not represent numbers that are close to one, two, and three for systems with single,

double, and triple bonds respectively. An important property of Mulliken's overlap population is that it possesses the correct rotational-hybridizational invariance that one should require for any quantity assigned a physical significance.

The researchers have compared the XPS and IR spectra for the most common synthetic corrosion products of zinc in NaCl environment. They found that the surface composition of the investigated synthetic oxidation products: ZnO, $Zn(OH)_2$, $Zn_5(OH)_8Cl_2{\cdot}H_2O$, $ZnCO_3$, and $Zn_5(CO_3)_2(OH)_6$, corresponds well with their stoichiometry despite the presence of surface contamination. Another important result was also that obtaining the standard spectra of pure ($Zn(OH)_2$ free) zinc oxide and other (ZnO-free) zinc hydroxyl compounds is in practice extremely difficult, even though the XRD phase analysis indicates the phase purity of these substances.

It has been shown that despite the complexity of the recorded photoelectron spectra, after the adoption of certain assumptions, one can estimate the corrosion products of zinc coatings [51].

Besides, there has been renewed interest in the wide-bandgap II–VI semiconductor ZnO, triggered by promising prospects for spintronic applications. Ferromagnetism was predicted for dilute magnetic doping. In a comprehensive investigation of ZnO thin films based on the combined measurement of macroscopic and microscopic properties, we find no evidence for carrier-mediated itinerant ferromagnetism. Superparamagnetism arises when phase separation or defect formation occurs, due to nanometer-sized metallic precipitates.

CONCLUSION

Considerable attention has recently been given to ZnO as a promising multifunctional material with wide-ranging technological applications. Understanding the interaction of water with ZnO is important for this material to be used in gas sensing, catalysis and biomedical applications. In summary, H_2O grabbing on the ZnO was investigated by first-principles calculations. We have provided ZnO nanocluster, then the geometrical parameters of H/OH adsorption on the surface of ZnO through the absorption status and current charge density were studied. ZnO–H_2O nanocluster indicates a larger isosurface map of electron delocalization due to labeling atoms of O1, Zn15, O27, H29, H30. A narrower connected area occupied by an isosurface map means that electron delocalization is relatively difficult. However, the large counter map of ELF for ZnO–H_2O can confirm that ZnO can be a promising semiconductor material for various applications.

ACKNOWLEDGEMENTS

In successfully completing this paper and its research, the author is grateful to Kastamonu Universi

REFERENCES

[1] S.Z. Zainabidinov, A.Y. Boboev, M.B. Rasulova, N.Y. Yunusaliyev. X-ray diffraction analysis, optical characteristics and electro-physical properties of the N-ZnO/P-NiO structure grown by the spray pyrolysis method. New Materials, Compounds and Applications. 8(3), 2024, 411-421. https://doi.org/10.62476/nmca83411

[2] S. Parmonov, K. Sharipov, D. Mirzavaliyev, F. Makhmudova, N. Askarova, R. Toshkodirova, N. Abdullaeva, M. Rifky, J.M. Harris, A. Kambarov. The technology of obtaining powders used in the production of solid alloys. New Materials, Compounds and Applications. 8(3), 2024, 450-458. https://doi.org/10.62476/nmca83450

[3] Monajjemi, M., Mohammadi, S., Shahriari, S. *et al.* Experimental and Theoretical Studies of ZnO Nanotubes: an Approach to Chemical Physics Characterization of ZnONTs, Including Morphology, Piezoelectric, and Density of States. *Russ. J. Phys. Chem. B* 18, 308–324 (2024). https://doi.org/10.1134/S1990793124010342

[4] Vasin, A.A., Dobryakov, A.L., Kochev, S.Y. *et al.* Relaxation of Multiple Excitons in ZnCdS and ZnCdS/ZnS Alloy Quantum Dots. *Russ. J. Phys. Chem. B* 18, 1646–1650 (2024). https://doi.org/10.1134/S1990793124701380

[5] Olkhovskaya, I.P., Krokhmal, I.I. & Glushchenko, N.N. Improvement of the Morphophysiological Parameters of Pepper after the Presowing Treatment of Seeds with Zinc Nanoparticles. *Russ. J. Phys. Chem. B* 18, 527–532 (2024). https://doi.org/10.1134/S1990793124020295

[6] I.I. Abbasov, M.A. Musayev, C.I. Huseynov, Q.Y. Eyyubov, N.N. Hasimova, A.J. Mammadova, A.A. Hadieva, Y.I. Aliyev, N.A. Qasumov, R.Sh. Rahimov. A study of impurity defect photoluminescence in ZnSe:Cr and ZnSe:Fe in the near infrared at room temperature. Advanced Physical Research. 5(3), 2023, 192-199

[7] Zhang, X.Q., Zhang, B. Effect of Pressure on the Structural, Mechanical, and Electronic Properties of Monoclinic $ZnWO_4$. *Russ. J. Phys. Chem. B* 17, 1049–1056 (2023). https://doi.org/10.1134/S1990793123050135

[8] Ikim, M.I., Spiridonova, E.Y., Gromov, V.F. *et al.* Effect of the Formation Method of $ZnO–In_2O_3$ Composites on Their Structural Characteristics and Conductivity. *Russ. J. Phys. Chem. B* 18, 283–288 (2024). https://doi.org/10.1134/S199079312401010X

[9] Zverev, A.S., Zvekov, A.A., Pugachev, V.M. *et al.* Controlling the Sensitivity of Pentaerythritol Tetranitrate to Visible Laser Radiation by the Addition of ZnO:Ag Nanopowder. *Russ. J. Phys. Chem. B* 17, 1135–1142 (2023). https://doi.org/10.1134/S1990793123050147

[10] Yuan, X., Tan, X. & Liu, B. Structural, Mechanical, Electronic and Optical Properties of Spinel $ZnAl_2O_4$ Underpressure from First-Principles Calculations. *Russ. J. Phys. Chem. B* 17, 886–895 (2023). https://doi.org/10.1134/S1990793123040322

[11] Martin, O.; González, V.; Tirado, M.; Comedi, D. Effects of methanol on morphology and photoluminescence in solvothermal grown ZnO powders and ZnO on Si. *Mater. Lett.* 2019, *251*, 41–44.

[12] Xiong, H.M.; Liu, D.P.; Xia, Y.Y.; Chen, J.S. Polyether-grafted ZnO Nanoparticles with Tunable and Stable Photoluminescence at Room Temperature. *Chem. Mater.* 2005, *17*, 3062–3064.

[13] Agarwal, D.C.; Singh, U.B.; Gupta, S.; Singhal, R.; Kulriya, P.K.; Singh, F.; Tripathi, A.; Singh, J.; Joshi, U.S.; Avasthi, D.K. Enhanced room temperature ferromagnetism and green photoluminescence in Cu doped ZnO thin film synthesised by neutral beam sputtering. *Sci. Rep.* 2019, *9*, 6675.

[14] Wolska, E.; Kaszewski, J.; Kiełbik, P.; Grzyb, J.; Godlewski, M.M.; Godlewski, M. Rare earth activated ZnO nanoparticles as biomarkers. *Opt. Mater.* 2014, *36*, 1655–1659

[15] Lim, J.H.; Kang, C.K.; Kim, K.K.; Park, I.K.; Hwang, D.K.; Park, S.J. UV

Electroluminescence Emission from ZnO Light-Emitting Diodes Grown by High-Temperature Radiofrequency Sputtering. *Adv. Mater.* 2006, *18*, 2720–2724.

[16] Tolubayeva, D.B.; Gritsenko, L.V.; Kedruk, Y.Y.; Aitzhanov, M.B.; Nemkayeva, R.R.; Abdullin, K.A. Effect of Hydrogen Plasma Treatment on the Sensitivity of ZnO Based Electrochemical Non-Enzymatic Biosensor. *Biosensors* 2023, *13*, 793. https://doi.org/10.3390/bios13080793

[17] Liu, H.; Zhang, Y.; Zhang, H.; Wang, L.; Wang, T.; Han, Z.; Wu, L.; Liu, G. Effect of plasma vitamin C levels on Parkinson's disease and age at onset: A Mendelian randomization study. *J. Transl. Med.* 2021, *19*, 221.

[18] Abdullin, K.A.; Gabdullin, M.T.; Gritsenko, L.V.; Ismailov, D.V.; Kalkozova, Z.K.; Kumekov, S.E.; Mukash, Z.O.; Sazonov, A.Y.; Terukov, E.I. Electrical, Optical, and Photoluminescence Properties of ZnO Films Subjected to Thermal Annealing and Treatment in Hydrogen Plasma. *Semiconductors* 2016, *50*, 1010–1014.

[19] Chang, S.-C.; Hu, J.-C.; Chan, H.-T.; Hsiao, C.-A. Influence of Processing Time in Hydrogen Plasma to Prepare Gallium and Aluminum Codoped Zinc Oxide Films for Low-Emissivity Glass. *Coatings* 2022, *12*, 945.

[20] Chang, S.-C.; Li, T.-H.; Chan, H.-T. Hydrogen Plasma Annealed Titanium Dioxide Oxide/Aluminum-doped Zinc Oxide Films Applied in Low Emissivity. Glass. *Int. J. Electrochem. Sci.* 2021, *16*, 210817.

[21] Zhang, C.; Cao, Z.; Zhang, G.; Yan, Y.; Yang, X.; Chang, J.; Song, Y.; Jia, Y.; Pan, P.; Mi, W.; et al. An electrochemical sensor based on plasma-treated zinc oxide nanoflowers for the simultaneous detection of dopamine and diclofenac sodium. *Microchem. J.* 2020, *158*, 105237.

[22] Srijita NundyAritra Ghosh*Tapas K. Mallick, Hydrophilic and Superhydrophilic Self-Cleaning Coatings by Morphologically Varying ZnO Microstructures for Photovoltaic and Glazing Applications. ACS Omega 2020, 5, 2, 1033–1039. https://doi.org/10.1021/acsomega.9b02758

[23] David Raymand, Adri C.T. van Duin, Daniel Spångberg, William A. Goddard III, Kersti Hermansson, Water adsorption on stepped ZnO surfaces from MD simulation, Surface Science, 604(9–10), 741–752 (2010). https://doi.org/10.1016/j.susc.2009.12.012

[24] Mollaamin, F., Monajjemi, M. Designing novel nanomaterials for Li-ion batteries: A physico-chemical study through hydrogen-powered horizons. New Materials, Compounds and Applications, 8(3), 303-323 (2024). https://doi.org/10.62476/nmca83303

[25] F. Mollaamin, M. Monajjemi, Application of nanoscale boron nitride for encapsulation of noxious transition metals (Cr, Mn, Fe, Zn, W, Cd) in soil: Physico-chemical characterization using DFT modeling. Advanced Physical Research. 7(1), 2025, 5-28. https://doi.org/10.62476/apr.7105

[26] Fatemeh Mollaamin, Majid Monajjemi, Determination of GaN nanosensor for scavenging of toxic heavy metal ions (Mn^{2+}, Zn^{2+}, Ag^{+}, Au^{3+}, Al^{3+}, Sn^{2+}) from water: Application of green sustainable materials by molecular modeling approach. Computational and Theoretical Chemistry. 1237, 114646, 2024. https://doi.org/10.1016/j.comptc.2024.114646

[27] Mollaamin, F., Monajjemi, M. Structural, Electromagnetic and Thermodynamic Analysis of Ion Pollutants Adsorption in Water by Gallium Nitride Nanomaterial: a Green Chemistry Application. *Russ. J. Phys. Chem. B* 18, 533–548 (2024). https://doi.org/10.1134/S199079312402012X

[28] Fatemeh Mollaamin, Majid Monajjemi, Trapping of toxic heavy metals from water by GN–nanocage: Application of nanomaterials for contaminant removal technique. Journal of Molecular Structure. 1300, 137214, 2024, https://doi.org/10.1016/j.molstruc.2023.137214.

[29] Mollaamin, F., Monajjemi, M. Tailoring and functionalizing the graphitic-like GaN and GaP nanostructures as selective sensors for NO, NO_2, and NH_3 adsorbing: a DFT study. *J Mol Model* 29, 170 (2023). https://doi.org/10.1007/s00894-023-05567-8

[30] F. Mollaamin, M. Monajjemi, In Silico-DFT Investigation of Nanocluster Alloys of Al-(Mg, Ge, Sn) Coated by Nitrogen Heterocyclic Carbenes as Corrosion Inhibitors, *J Clust Sci*, 34 (6), 2901–2918,

2023. https://doi.org/10.1007/s10876-023-02436-5

[31] Mollaamin, F.; Monajjemi, M. Doping of Graphene Nanostructure with Iron, Nickel and Zinc as Selective Detector for the Toxic Gas Removal: A Density Functional Theory Study. *C* 2023, *9*, 20. https://doi.org/10.3390/c9010020

[32] F. Mollaamin, M. Monajjemi, Transition metal (X = Mn, Fe, Co, Ni, Cu, Zn)-doped graphene as gas sensor for CO_2 and NO_2 detection: A molecular modeling framework by DFT perspective, *J. Mol. Model.,* 29(4), 119, 2023. https://doi.org/10.1007/s00894-023-05526-3

[33] F. Mollaamin, S. Shahriari, M. Monajjemi, Z. Khalaj, Nanocluster of Aluminum Lattice via Organic Inhibitors Coating: A Study of Freundlich Adsorption, *J. Clust. Sci.,* 34(3), 1547–1562, 2023. https://doi.org/10.1007/s10876-022-02335-1

[34] Mollaamin, F., Monajjemi, M. In Situ Ti-Embedded SiC as Chemiresistive Nanosensor for Safety Monitoring of CO, CO_2, NO, NO_2: Molecular Modelling by Conceptual Density Functional Theory. *Russ. J. Phys. Chem. B* 18, 49–66 (2024). https://doi.org/10.1134/S1990793124010159

[35] Mollaamin, F., Monajjemi,M., Adsorption ability of Ga_5N_{10} nanomaterial for removing metal ions contamination from drinking water by DFT, Int J Quantum Chem, 2024, 124, e27348. https://doi.org/10.1002/qua.27348.

[36] Mollaamin F and Monajjemi M. Molecular modelling framework of metal-organic clusters for conserving surfaces: Langmuir sorption through the TD-DFT/ONIOM approach. Molecular Simulation 2023; 49(4): 365–376. https://doi.org/10.1080/08927022.2022.2159996.

[37] Mollaamin, F. Competitive Intracellular Hydrogen-Nanocarrier Among Aluminum, Carbon, or Silicon Implantation: a Novel Technology of Eco-Friendly Energy Storage using Research Density Functional Theory. Russ. J. Phys. Chem. B 18, 805–820 (2024). https://doi.org/10.1134/S1990793124700131

[38] Frisch, M. J.; Trucks, G. W.; Schlegel, H. B.; Scuseria, G. E.; Robb, M. A.; et al. Gaussian 16, Revision C.01, Gaussian, Inc., Wallingford CT, 2016.

[39] GaussView, Version 6.06.16, Dennington, Roy; Keith, Todd A.; Millam, John M. Semichem Inc., Shawnee Mission, KS, 2016.

[40] Zihan Xu, Chenglong Qin, Yushu Yu, Gang Jiang, Liang Zhao, First-principles study of adsorption, dissociation, and diffusion of hydrogen on α-U (110) surface. AIP Advances 14, 055114 (2024). https://doi.org/10.1063/5.0208082

[41] T. Lu & F. Chen, Multiwfn: A multifunctional wavefunction analyzer. J. Comput. Chem. 33, 580–592 (2012). doi.org/10.1002/jcc.22885

[42] T. Lu, A comprehensive electron wavefunction analysis toolbox for chemists, Multiwfn. J. Chem. Phys. 161, 082503 (2024). doi.org/10.1063/5.0216272

[43] Mollaamin, F., Monajjemi, M. Perspective of Clean Energy-saving by Semiconducting Quantum Dot Nanomaterials through Photoelectric and Density of States Analysis. *J Fluoresc* (2025). https://doi.org/10.1007/s10895-025-04207-z

[44] Steinmann,S.N. Mob, Y. Corminboeuf,C. How do electron localization functions describe π-electron delocalization? Phys. Chem. Chem. Phys. 13(2011)20584-20592. https://doi.org/10.1039/C1CP21055F

[45] Tian, L. Feiwu, C. Xuebao, W. Meaning and Functional Form of the Electron Localization Function, Acta Phys. Chim. Sin. 27 (2011) 2786–2792. https://doi.org/10.3866/PKU.WHXB20112786

[46] M.F. Thanoon, L.M. Al-Nema, Hardness, elastic modulus, water solubility and Fourier Transformation Infrared (FTIR) of the modified soft liner with two types of plasticizers. New Materials, Compounds and Applications. 8(2), 2024, 233-243 https://doi.org/10.62476/nmca82233

[47] I. Mayer, Improved definition of bond orders for correlated wave functions. Chemical Physics Letters 544, 83-86 (2012). https://doi.org/10.1016/j.cplett.2012.07.0

[48] Mollaamin, F. and Monajjemi, M. (2023), Graphene-based resistant sensor decorated with Mn, Co, Cu for nitric oxide detection: Langmuir adsorption & DFT method. Sensor Review. 43(4), 266-279. https://doi.org/10.1108/SR-03-2023-0040

[49] Tian Lu and Feiwu Chen, Bond Order Analysis Based on the Laplacian of

Electron Density in Fuzzy Overlap Space. J. Phys. Chem. A 2013, 117, 14, 3100–3108. https://doi.org/10.1021/jp4010345

[50] S.H.M. Sheet, R.B. Mahmod, N.H.M. Saeed, S.M. Saied, Theoretical study for comparison of pKa of a number of Achiff bases by employing parameters derived from DFT and MP2 method. New Materials, Compounds and Applications. 8(1), 2024, 94-108. https://doi.org/10.62476/nmca8194

[51] Juliusz Winiarski, Włodzimierz Tylus, Katarzyna Winiarska, Irena Szczygieł, Bogdan Szczygieł, XPS and FT-IR Characterization of Selected Synthetic Corrosion Products of Zinc Expected in Neutral Environment Containing Chloride Ions. HindawiJournal of Spectroscopy, 2018, 2079278. https://doi.org/10.1155/2018/2079278